

Supporting Information

Block Polymer Membranes Functionalized with Nanoconfined Polyelectrolyte Brushes Achieve Sub-Nanometer Selectivity

Yizhou Zhang,[†] Ryan A. Mulvenna,[‡] Siyi Qu,[†] Bryan W. Boudouris,^{‡,§} and William A. Phillip^{†,*}

[†] Department of Chemical and Biomolecular Engineering, University of Notre Dame, Notre Dame, Indiana 46556, United States

[‡] Charles D. Davidson School of Chemical Engineering and [§] Department of Chemistry, Purdue University, West Lafayette, Indiana 47907, United States.

* To whom correspondence should be addressed: wphillip@nd.edu

Detailed Experimental Procedure

Block Polymer Synthesis.

All reagents were purchased from Sigma-Aldrich and used as received unless otherwise noted. The polyisoprene-*b*-polystyrene-*b*-poly(*N,N*-dimethylacrylamide) (PI-PS-PDMA) block polymer used in this study was synthesized using a controlled reversible addition-fragmentation chain transfer (RAFT) polymerization technique following previously-reported protocols.¹⁻² Using this technique, the polyisoprene (PI), polyisoprene-*b*-polystyrene (PI-PS), and PI-PS-PDMA polymers were synthesized sequentially using isoprene, styrene, and *N,N*-dimethylacrylamide, as monomers, respectively. The monomers were purified by passage through a basic alumina (Fisher Scientific) packed column twice prior to immediate use. Degassed, inhibitor-free tetrahydrofuran (THF), which was used as a co-solvent in the polymerization of PI-PS-PDMA from the PI-PS macroinitiator, was purified by passing through an alumina column (Innovative Technology) before immediate use. The ¹H nuclear magnetic resonance (NMR) spectroscopy data were acquired on a Bruker Advance-III-800 spectrometer, and these data were used to evaluate the molecular weights for the block polymer moieties after each step of the triblock polymerization scheme. The NMR samples were prepared by dissolving the polymers in deuterated chloroform at a

concentration of ~1% (by weight). The dispersity values (\mathcal{D}) of the homopolymer PI, the diblock polymer PI-PS, and the PI-PS-PDMA triblock polymer were measured using a Hewlett-Packard 1260 Infinity series size-exclusion chromatography (SEC) that was equipped with a Hewlett-Packard G1362A refractive index (RI) detector and three PLgel 5 μm MIXED-C columns. During the SEC measurements, the mobile phase consisted of THF at 35 °C flowing at a volumetric flow rate of 1 mL min⁻¹. Polystyrene samples (Agilent Easi Cal) were used as standards for the calibration. The PI-PS-PDMA block polymer used in this study had a number averaged molecular weight (M_n) of 75 kg mol⁻¹, a dispersity of 1.35, and volume fraction values of $f_{\text{PI}} = 0.25$, $f_{\text{PS}} = 0.42$, and $f_{\text{PDMA}} = 0.33$.

Hollow Fiber Membrane Fabrication.

Membranes were cast in a fume hood situated in an air-conditioned room with the temperature regulated at ~23°C and with the relative humidity ranging from 30% to 60%. The membrane casting solution was prepared by dissolving 4% (by weight) PI-PS-PDMA block polymer into a binary solvent mixture of THF and 1,4-dioxane at a ratio of 3:7 (by weight). The dual-layer block polymer hollow fiber membrane was fabricated by using the dip-coating and SNIPS methodology as previously reported.³ The coating was performed by using a customized Teflon coating mold. This mold had a cylindrical opening at the bottom, and was used as a polymer solution reservoir during the coating process. That is, the polymer solution was pipetted into the mold until a ~1 cm deep pool was formed. A poly(vinylidene fluoride) (PVDF) ultrafiltration hollow fiber membrane (kindly provided by The Dow Chemical Company, and with a nominal pore size of 30 nm), which was used as a mechanical support for the block polymer layer, was threaded through the opening and pulled vertically through the pool of solution at a uniform speed of 5 mm s⁻¹. Because the cylindrical opening of the mold had a diameter comparable to that of the

PVDF hollow fiber (both are ~1.2 mm), the polymer solution did not leak during the coating process. A constant solvent evaporation time of 40 s was used for the entire length of hollow fiber before it was immersed in the non-solvent (DI water) bath.

Membrane Hydrolysis and Functionalization with Carbodiimide Coupling Reaction.

The solid-state hydrolysis that converted the self-assembled PI-PS-PDMA of the dual layer hollow fiber into polyisoprene-*b*-polystyrene-*b*-poly(acrylic acid) (PI-PS-PAA) followed a similar protocol as detailed in previous work.² The PI-PS-PDMA membrane was fully immersed in a bath of 6 M hydrochloric (HCl) acid that was then heated to 80 °C for 28 h. After this time, the heat source was turned off, and the hot acid bath was allowed to cool to room temperature overnight. The PI-PS-PAA membrane was then removed from the acid bath, rinsed thoroughly with DI water, and the nanoporous thin film was stored in a DI water bath prior to further functionalization reactions. A Bruker Tensor 27 Fourier-transformed Infrared (FTIR) spectrometer equipped with a diamond lens attenuated total reflectance (ATR) module was used to analyze the chemical composition of the hydrolyzed membrane, and the ATR-FTIR spectra was collected in 64 scans over a range of $400 \leq \nu \leq 4,000 \text{ cm}^{-1}$.

The PAA polymer brushes that lined the pore walls of the PI-PS-PAA membrane were converted to poly(2-acrylamido-ethane-1,1-disulfonic acid) (PADSA) via a carbodiimide coupling reaction that used 1-ethyl-3-(3-dimethylaminopropyl) carbodiimide hydrochloride (EDC·HCl) as the carboxyl activating agent, following a previous reported protocol.⁴ Pieces of a PI-PS-PAA membrane were placed in an aqueous solution containing 5 mM EDC·HCl (Chem-Impex International, Inc.), 25 mM hydroxybenzotriazole (HOBt), 25 mM ammonium 2-aminoethane-1,1-disulfonic acid (Strem Chemicals Inc.), 500 mM NaCl, and 100 mM 2-(4-morpholino)-ethanesulfonic acid (MES, Fisher Scientific). The reaction mixture was left at room temperature

for 48 h. Following the reaction, the PI-PS-PADSA membrane was removed from the solution and was rinsed with DI water overnight. The pore lining chemistry of PI-PS-PADSA was analyzed using the Bruker Tensor 27 ATR-FTIR spectrometer with the same operating parameters as described above. Both the PI-PS-PAA and PI-PS-PADSA hollow fiber membranes were stored in DI water before they were assembled into custom-built hollow fiber membrane modules, which were operated in an outside-to-inside configuration (i.e., the pressurized feed was flowing through the outside and passing through the membrane surface to the inside of the hollow fiber membranes).

Imaging Analysis and Elemental Mapping.

A Magellan 400 (FEI Company) Digital Field Emission Scanning Electron Microscope (FE-SEM) equipped with an Energy Dispersive X-Ray Spectrometer (EDS, Bruker) was used to characterize the nanoscale morphology and elemental composition of the PI-PS-PADSA dual-layer membrane. For surface characterization, samples of the air-dried composite membrane were cut into small pieces of ~0.3 cm length from longer pieces using a razor blade. For cross-sectional analysis, dried samples were cryo-fractured after submerging them in a bath of liquid nitrogen for ~20 s. During SEM imaging, the samples were mounted on standard SEM pin stub (Ted Pella, Inc.) by using carbon tape, and were sputter-coated with ~2.0 nm of iridium prior to loading them into the microscope. SEM micrographs were captured using a working distance of ~4 mm, a beam current of 13 pA, and accelerating voltages that ranged from 3 to 5 kV. To estimate the dry-state pore size and the porosity of the membranes, the collected micrographs were further processed using the ImageJ software package.⁵ During the EDS elemental mapping, the samples were mounted on a SEM pin stub with 90° mount and sputter-coated with ~2.0 nm of iridium prior to loading the pin stub into the microscope. The EDS maps were recorded at working distance of ~4.7 mm, a beam current of 1.6 nA, and an accelerating voltage of 5kV.

Transport Characterization.

The composite hollow fiber membranes were assembled into customized hollow fiber modules that operated in an outside-to-inside configuration. The hollow fibers in the module had an effective filtration length of ~ 2 cm that corresponded to an effective membrane surface area of ~ 0.7 cm². The transport characterization was operated by attaching the hollow fiber module to a closed-loop cross-flow filtration setup. The feed solution was stored in an 800 mL cell reservoir (EMD Millipore, Amicon 6028), and it was recirculated through the system using a gear pump drive (Cole-Parmer). A well-regulated transmembrane pressure ranging from 5 to 55 psi was applied for solute rejection and hydraulic permeability characterization experiments using nitrogen gas. The solution that permeated through the membrane was collected in a scintillation vial that rested on an electronic balance. The mass of the vial was logged electronically every 30 s for up to 5 hours to acquire a stable and accurate flux. Between each of the transport experiments, the storage tank was emptied and the filtration system was rinsed thoroughly with DI water or salt solution at least three times.

The molecular weight cut-off (MWCO) experiments were performed using molecules with known sizes in order to characterize the size-selective solute separation performance of the membranes. Sucrose and poly(ethylene oxide) (PEO) molecules (Polymer Source) with number averaged molecular weights of 0.60, 1.1, 2.1, 4.0 and 6.0 kg mol⁻¹ and dispersity values of 1.10 or less were used as solutes. To prepare the feed solution, a single solute at a concentration of ~ 0.6 g L⁻¹ was dissolved in DI water, 10 mM NaCl, or 10 mM MgCl₂. The solution pH was not adjusted during the MWCO experiments. The solution pH for solutes dissolved in DI water was ~ 5.5 and the pH for solutes dissolved in the salt solution was ~ 7 . During the rejection experiments, the feed solution on the shell side of the hollow fiber membrane was set at a superficial velocity of ~ 0.3 m s⁻¹ to reduce the effects of concentration polarization. A total organic carbon analyzer (TOV-VCSH,

Shimadzu) was used to quantify the concentration of solute molecules in the feed and permeate solutions. The percent rejection [$R(\%)$] was then calculated by comparing the solute concentration in the feed and permeate solutions by the following equation.

$$R(\%) = 100\% \times \left(1 - \frac{C_p}{C_f}\right) \quad (\text{S1})$$

Here, C_p is the concentration of the permeate, and the C_f corresponds to the concentration of the feed solution. To account for the intrinsic solute separation of the membrane, the observed percent rejection was adjusted for the effect of concentration polarization.⁶⁻⁷ The ratio of the water flux, j_w , to the mass transfer coefficients, k , that is produced by the cross-flow configuration was smaller than 0.1. Therefore, there was no significant concentration polarization during the filtration experiment. To compare the experimental MWCO with theory, the work established by Zeman and Wales that connects the pore size of an ideal membrane (e.g., with a well-defined pore size) with the percent rejection, [$R(\%)$], of a solute with a known size was implemented. This theory is based on the assumption that no concentration polarization exists.⁸

$$R(\%) = 1 - [(1 - \lambda)^2 [2 - (1 - \lambda)^2] \exp(-0.7146\lambda^2)] \quad (\text{S2})$$

Where λ is the ratio of characteristic solute diameter to the pore diameter.

The pH-responsive hydraulic permeability of membranes was measured using pH-adjusted aqueous solutions as the feed. The solution pH was adjusted by adding 1 M NaOH or 1 M HCl as needed to a Nalgene bottle containing 3.5 L of solution. An Accumet AP115 portable pH meter (Fisher scientific) and paper pH test strips (Fisher scientific) were used to measure the pH of the solution prior to use. The response of hydraulic permeability to changes in ionic strength was characterized using pH-unadjusted salt solutions of varying concentrations. The salt solution was prepared by dissolving a single salt NaCl or MgCl₂ into DI water at the prescribed concentration.

A 0.45 μm syringe filter (EMD Millipore) was used to filter impurities from 100 mM and 500 mM MgCl_2 solution prior the salt solution was transferred into the 800 mL cell reservoir.

Calculation for the Osmotic to Salted Brush Transition.

The response of polyelectrolyte brushes in solutions containing monovalent or multivalent cations is well-studied, and the transition of polymer brushes from the osmotic brush regime to salted brush regime has been probed experimentally in prior work.⁹⁻¹⁴ In the osmotic brush regime, the thickness of the extended brush does not depend on the concentration of ions in solution. In the salted brush regime, the brush thickness has a power law dependence on the concentration of ions in solution with a $-1/3$ exponent. It is likely that the high grafting density and high surface charge density of the materials demonstrated in this study shifts the transition between these two regimes towards higher ionic strengths. The following equation is used to estimate where this transition occurs,⁹

$$c^* = \frac{\alpha N \sigma}{R N_A} \quad (\text{S3})$$

where α is the fraction of free counter ions within the polymer brushes, N is the number of repeat units in the polymer brushes lining the pore wall, σ is the areal density of brushes, R is the pore radius, and N_A is Avogadro's number. In the case of the PADSAs brush, using $N = 250$, $\sigma = 0.7$ brushes nm^{-2} , $R = 17$ nm, and assuming a value of α between 0.15 and 0.4, it is expected the transition to occur at a concentration between 2.5 M and 6.8 M. Below this concentration, the polymer brushes remain in the osmotic brush regime and their length does not depend on salt concentration. This might explain why the collapse of the polyelectrolyte brushes was not significant in the hydraulic permeability experiments for either the PI-PS-PADSAs membranes (in NaCl or MgCl_2) or the PI-PS-PAA (in NaCl).

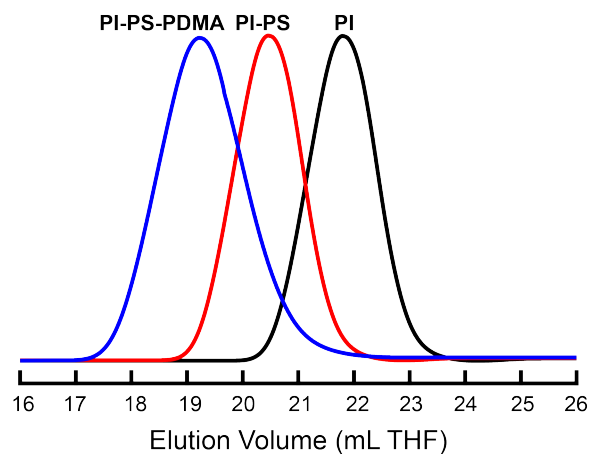


Figure S1. SEC traces of the RAFT-polymerized constituent PI homopolymer and PI-PS diblock copolymers, and the SEC trace of the final PI-PS-PDMA triblock polymer sample used in the hollow fiber membrane casting.

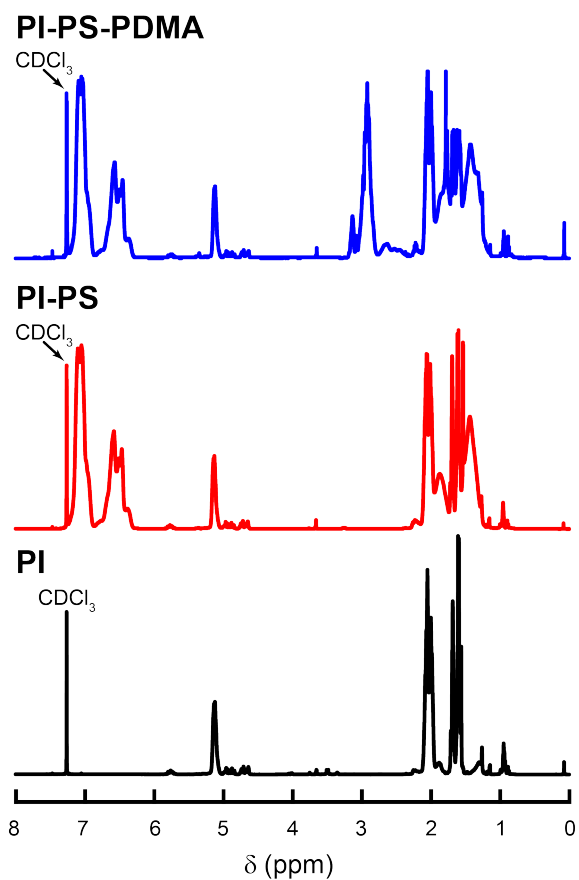


Figure S2. ^1H NMR spectra of the RAFT-polymerized constituent PI homopolymer and PI-PS diblock copolymer, and the spectrum of the final PI-PS-PDMA triblock polymer sample used in the hollow fiber membrane casting.

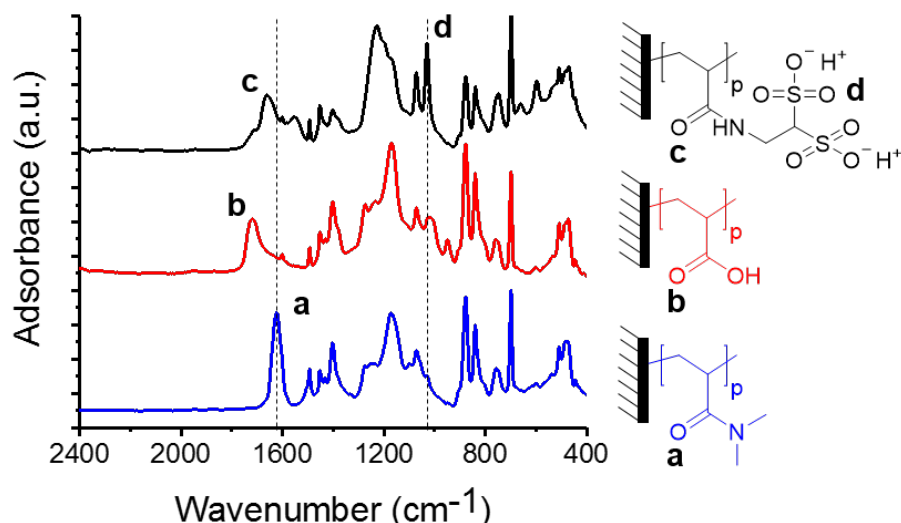


Figure S3. ATR-FTIR spectra confirmed the solid-state conversion of the pore wall lining functional groups from PDMA to PADSA. First, the parent PI-PS-PDMA membrane was immersed in an aqueous 6 M HCl solution at 80 °C for 28 h to convert PDMA to PAA. The disappearance of the amide carbonyl group at $\sim 1630\text{ cm}^{-1}$ (labeled as **a**) and the appearance of the carbonyl peak at $\sim 1720\text{ cm}^{-1}$ (labeled as **b**), which is associated with carboxylic acids, from the bottom to middle spectra are indicative of the successful conversion. The PI-PS-PAA membrane was then functionalized with 2-aminoethane-1,1-disulfonic acid at room temperature using a carbodiimide coupling reaction to produce the PI-PS-PADSA membrane in 48 h. The success of this coupling reaction was demonstrated by the shift of the carbonyl peak to $\sim 1660\text{ cm}^{-1}$ (labeled as **c**) and the appearance of two characteristic peaks associated with sulfonate at $\sim 1030\text{ cm}^{-1}$ (labeled as **d**) in the top spectrum. An estimation of percent conversion from PAA to PADSA is calculated from the relative characteristic peak areas collected prior and after the coupling reaction, which suggests the reaction achieves $\sim 90\%$ conversion within 48 h.

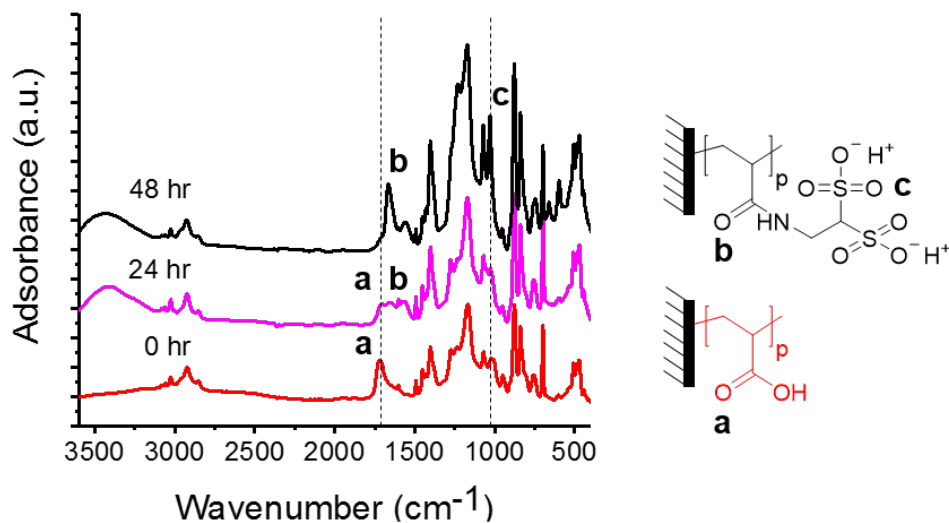


Figure S4. ATR-FTIR spectra taken at different time points during the solid-state conversion of the pore wall lining chemistry from PAA to PADSA. The reaction was performed by immersing pieces of a PI-PS-PAA membrane in a carbodiimide coupling solution containing 5 mM 1-ethyl-3-(3-dimethylaminopropyl) carbodiimide hydrochloride (EDC·HCl), 25 mM hydroxybenzotriazole (HOBt) and 25 mM ammonium 2-aminoethane-1,1-disulfonic acid at room temperature for 48 h. The membrane samples were removed from the coupling solution, rinsed with DI water overnight, and dried in a vacuum oven for 24 h prior to the FTIR analysis. As shown in the spectra, the intensity of the carbonyl peak at $\sim 1720\text{ cm}^{-1}$ (labeled as **a**), which is associated with carboxylic acids, decreased as the PAA is converted to PADSA. The success of this coupling reaction was further confirmed by the gradual appearance of the carbonyl peak at $\sim 1660\text{ cm}^{-1}$ (labeled as **b**), which is associated with amide bonds, and the sulfonic acid peaks at $\sim 1030\text{ cm}^{-1}$ (labeled as **c**). The percent conversion of PAA to PADSA was assessed from the integrated peak areas retrieved from the FTIR spectra, and $> 90\%$ conversion is determined 48 h after the reaction is initiated.

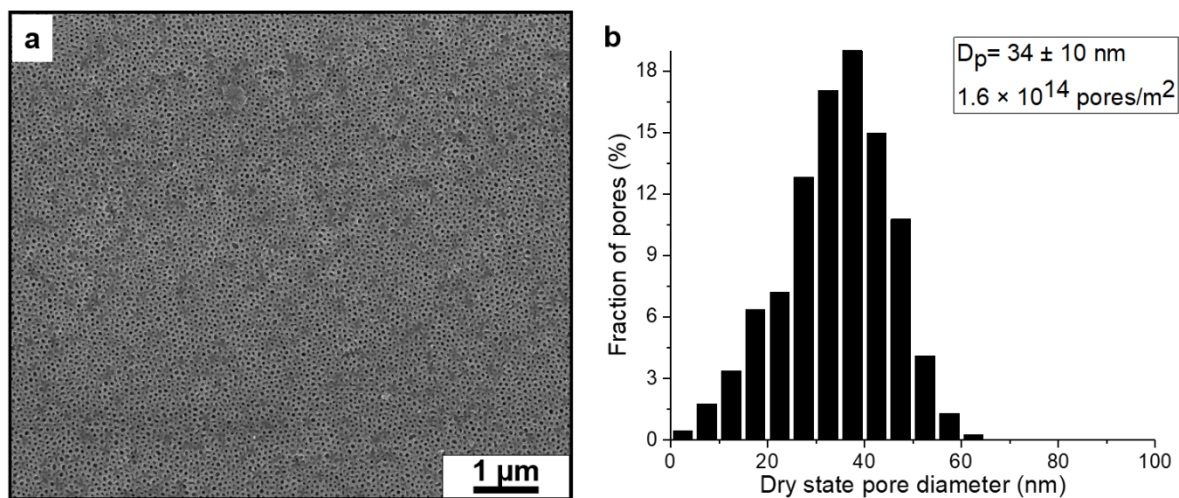


Figure S5. (a) An SEM micrograph of the nanostructure observed on the top active layer of the block polymer membrane, and (b) corresponding pore size distribution obtained using the ImageJ software package. The membrane had a well-defined surface nanostructure with a dry-state pore size as 34 ± 10 nm and a porosity of 1.6×10^{14} pores m^{-2} . It is important to note that, prior environmental atomic force microscopy (AFM) analysis have demonstrated that, when hydrated, the pore-walling lining polymer brushes assume a more extended conformation.² The extension likely sharpens the effective pore size distribution and gives rise to high solute selectivity (e.g., during the solute rejection tests).

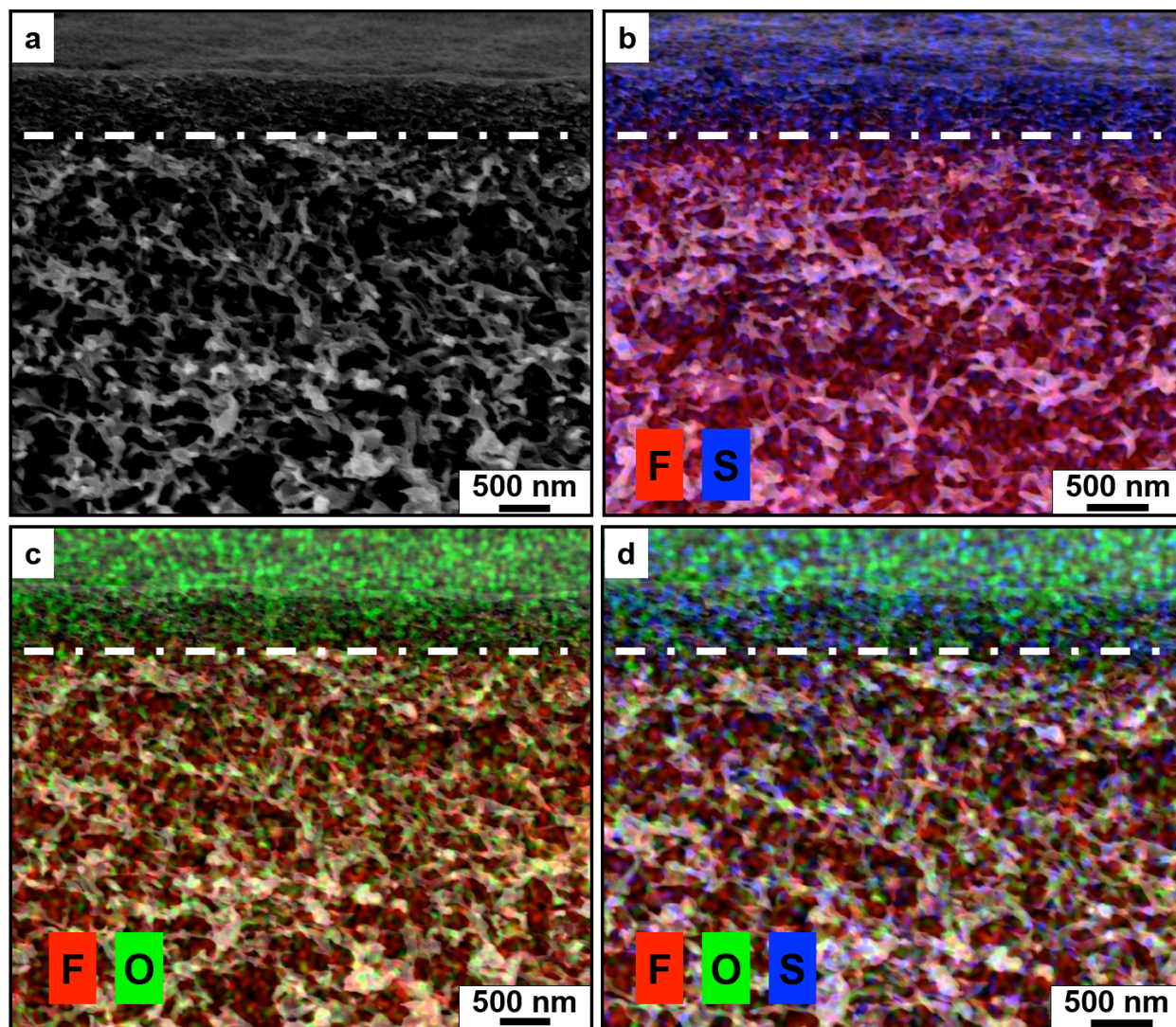


Figure S6. (a) SEM micrograph of the PI-PS-PADSA membrane cross-section. The 500 nm-thick block polymer layer is supported by a macroporous PVDF substrate. EDS elemental maps of the membrane cross-section demonstrated the abundance of (b) fluoride and sulfur, (c) fluoride and oxygen, and (d) fluoride, sulfur and oxygen. The oxygen-rich and sulfur-rich regions are confined to the 500 nm-thick block polymer layer while the fluoride-rich region only appears within the supporting substrate.

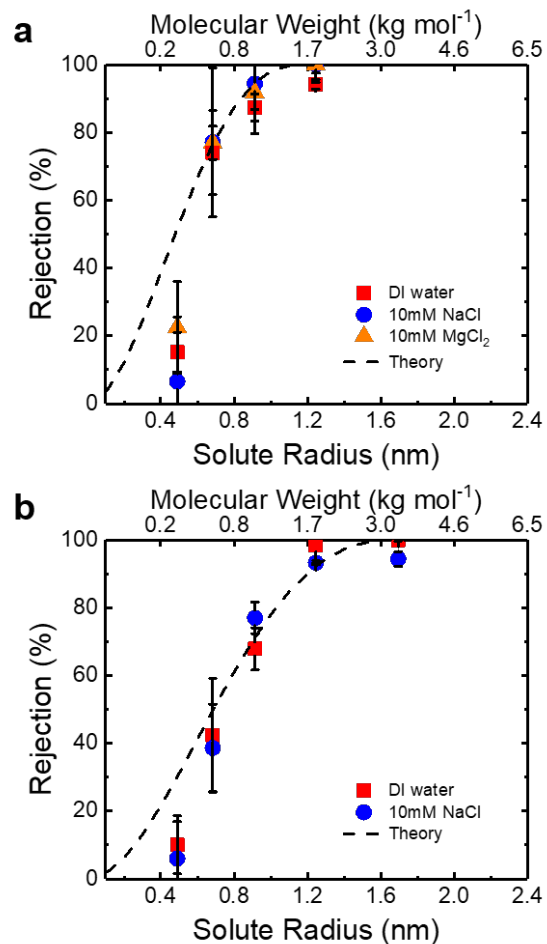


Figure S7. A comparison between the experimental solute rejection performance of the (a) PI-PS-PADSA and (b) PI-PS-PAA hollow fiber membranes to the performance predicted by theory. The theoretical MWCO curves for the PI-PS-PADSA and PI-PS-PAA membranes were developed based on ideal membranes (i.e., with a single well-defined pore size) with pore diameters of 2.3 nm and 3.4 nm, respectively.

References

1. Mulvenna, R. A.; Prato, R. A.; Phillip, W. A.; Boudouris, B. W. Polymerization Rate Considerations for High Molecular Weight Polyisoprene-b-Polystyrene-b-Poly (N, N-dimethylacrylamide) Triblock Polymers Synthesized Via Sequential Reversible Addition-Fragmentation Chain Transfer (RAFT) Reactions. *Macromol. Chem. Phys.* **2015**, *216* (17), 1831-1840.
2. Mulvenna, R. A.; Weidman, J. L.; Jing, B.; Pople, J. A.; Zhu, Y.; Boudouris, B. W.; Phillip, W. A. Tunable nanoporous membranes with chemically-tailored pore walls from triblock polymer templates. *J. Membr. Sci.* **2014**, *470*, 246-256.
3. Zhang, Y.; Mulvenna, R. A.; Boudouris, B. W.; Phillip, W. A. Nanomanufacturing of high-performance hollow fiber nanofiltration membranes by coating uniform block polymer films from solution. *J. Mater. Chem. A* **2017**, *5* (7), 3358-3370.
4. Rzyayev, J.; Hillmyer, M. A. Nanochannel Array Plastics with Tailored Surface Chemistry. *J. Am. Chem. Soc.* **2005**, *127* (38), 13373-13379.
5. Schneider, C. A.; Rasband, W. S.; Eliceiri, K. W. NIH Image to ImageJ: 25 years of Image Analysis. *Nat. Methods* **2012**, *9*, 671-675.
6. Mehta, A.; Zydney, A. L. Permeability and selectivity analysis for ultrafiltration membranes. *J. Membr. Sci.* **2005**, *249* (1), 245-249.
7. Yang, M.; Cussler, E. L. Designing hollow-fiber contactors. *AIChE J.* **1986**, *32* (11), 1910-1916.
8. Zeman, L. J.; Wales, M. Polymer Solute Rejection by Ultrafiltration Membranes. In *Synthetic Membranes: Vol. II*, American Chemical Society: Washington, DC, 1981; Vol. 154, pp 411-434.
9. Li, F.; Balastre, M.; Schorr, P.; Argillier, J.-F.; Yang, J.; Mays, J. W.; Tirrell, M. Differences between Tethered Polyelectrolyte Chains on Bare Mica and Hydrophobically Modified Mica. *Langmuir* **2006**, *22* (9), 4084-4091.
10. Yu, J.; Mao, J.; Yuan, G.; Satija, S.; Jiang, Z.; Chen, W.; Tirrell, M. Structure of Polyelectrolyte Brushes in the Presence of Multivalent Counterions. *Macromolecules* **2016**, *49* (15), 5609-5617.
11. Balastre, M.; Li, F.; Schorr, P.; Yang, J.; Mays, J. W.; Tirrell, M. V. A study of Polyelectrolyte Brushes Formed from Adsorption of Amphiphilic Diblock Copolymers Using the Surface Forces Apparatus. *Macromolecules* **2002**, *35* (25), 9480-9486.
12. Willott, J. D.; Murdoch, T. J.; Humphreys, B. A.; Edmondson, S.; Webber, G. B.; Wanless, E. J. Critical Salt Effects in the Swelling Behavior of a Weak Polybasic Brush. *Langmuir* **2014**, *30* (7), 1827-1836.
13. Chu, X.; Yang, J.; Liu, G.; Zhao, J. Swelling enhancement of polyelectrolyte brushes induced by external ions. *Soft Matter* **2014**, *10* (30), 5568-5578.
14. Wu, T.; Gong, P.; Szleifer, I.; Vlček, P.; Šubr, V.; Genzer, J. Behavior of Surface-Anchored Poly(acrylic acid) Brushes with Grafting Density Gradients on Solid Substrates: 1. Experiment. *Macromolecules* **2007**, *40* (24), 8756-8764.